Bohayra Mortazavi, Obaidur Rahaman, Arezoo Dianat, Timon Rabczuk

Mechanical responses of borophene sheets: a first-principles study

Erstveröffentlichung in / First published in:
Physical chemistry, chemical physics. 2016, 18(39), S. 27405 - 27413 [Zugriff am: 04.11.2019]. Royal Society of Chemistry. ISSN 1463-9084.

DOI: https://doi.org/10.1039/c6cp03828j

PCCP

PAPER

View Article Online
View Journal | View Issue

Cite this: *Phys. Chem. Chem. Phys.*, 2016, **18**, 27405

Mechanical responses of borophene sheets: a first-principles study

Bohayra Mortazavi,*[a] Obaidur Rahaman,[a] Arezoo Dianat[b] and Timon Rabczuk[a]

Received 2nd June 2016,
Accepted 2nd September 2016

DOI: 10.1039/c6cp03828j

www.rsc.org/pccp

Recent experimental advances for the fabrication of various borophene sheets introduced new structures with a wide range of applications. Borophene is the boron atom analogue of graphene. Borophene exhibits various structural polymorphs all of which are metallic. In this work, we employed first-principles density functional theory calculations to investigate the mechanical properties of five different single-layer borophene sheets. In particular, we analyzed the effect of the loading direction and point vacancy on the mechanical response of borophene. Moreover, we compared the thermal stabilities of the considered borophene systems. Based on the results of our modelling, borophene films depending on the atomic configurations and the loading direction can yield a remarkable elastic modulus in the range of 163–382 GPa nm and a high ultimate tensile strength from 13.5 GPa nm to around 22.8 GPa nm at the corresponding strain from 0.1 to 0.21. Our study reveals the remarkable mechanical characteristics of borophene films.

1. Introduction

Over the last couple of decades, there have been tremendous efforts for the fabrication of two-dimensional (2D) materials. 2D materials are currently considered among the most interesting research topics because of their remarkable and wide range of potential applications. Interest toward this new class of materials originated from the successful production of graphene,[1–3] and the honeycomb lattice of carbon atoms in a planar form. Graphene is a semi-metallic material which exhibits exceptional mechanical[4] and heat conduction[5] properties. After the synthesis of graphene, other 2D materials were successfully fabricated such as hexagonal boron-nitride,[6,7] graphitic carbon nitride,[8] silicene,[9,10] germanene,[11] stanene[12] and transition metal dichalcogenides[13–15] like molybdenum disulfide (MoS_2). Nevertheless, interest toward the synthesis and application of 2D materials sounds to be enhancing. In line with the continuous advances in the fabrication of new 2D materials, exciting developments have recently taken place with respect to the synthesis of borophene.[16,17] To the best of our knowledge, three different 2D boron films have been experimentally fabricated so far all by epitaxial growth of boron atoms on a silver substrate.[16,17] In accordance with theoretical predictions,[18,19] these sheets present metallic properties. For the real application of these new films, a comprehensive understanding of their properties plays a critical role. In this regard, theoretical studies can be considered as promising approaches to assess the properties of these materials that are difficult, expensive and time consuming to be experimentally evaluated.[20–28] One of the key factors for the application of a material is its mechanical properties that correspond to the stability of the material under the applied mechanical strains. In this work we therefore studied the mechanical properties of five different borophene sheets using first-principles density functional theory (DFT) calculations. We elaborately studied the effect of the loading direction and defect formation on the mechanical properties of different borophene sheets.

2. Atomistic modelling

In this study, we investigated the mechanical properties of five different boron sheets (S1–S5) which are illustrated in Fig. 1. To probe the effect of the loading direction, we analyzed the mechanical properties along the armchair and zigzag directions as depicted in Fig. 1. All constructed samples were periodic in the planar directions therefore the obtained results correspond to infinite sheets and not borophene nanoribbons. Sheet S1 is the densest structure with out of plane buckling, which was synthesised experimentally by Mannix *et al.*[16] Sheets S2 and S3 are planar borophene sheets that have been most recently experimentally fabricated by Feng *et al.*[17] In addition we considered two other sheets that have been theoretically predicted.[29] In this study, we used relatively large atomic models with 75 atoms to 128 atoms. DFT calculations were performed as implemented in the Vienna *ab initio* simulation package (VASP)[30,31] using the Perdew–Burke–Ernzerhof

[a] *Institute of Structural Mechanics, Bauhaus-Universität Weimar, Marienstr. 15, D-99423 Weimar, Germany. E-mail: bohayra.mortazavi@gmail.com, amieor@gmail.com, timon.rabczuk@uni-weimar.de; Fax: +49 364 358 4511; Tel: +49 157 8037 8770*

[b] *Institute for Materials Science and Max Bergman Center of Biomaterials, TU Dresden, 01062 Dresden, Germany*

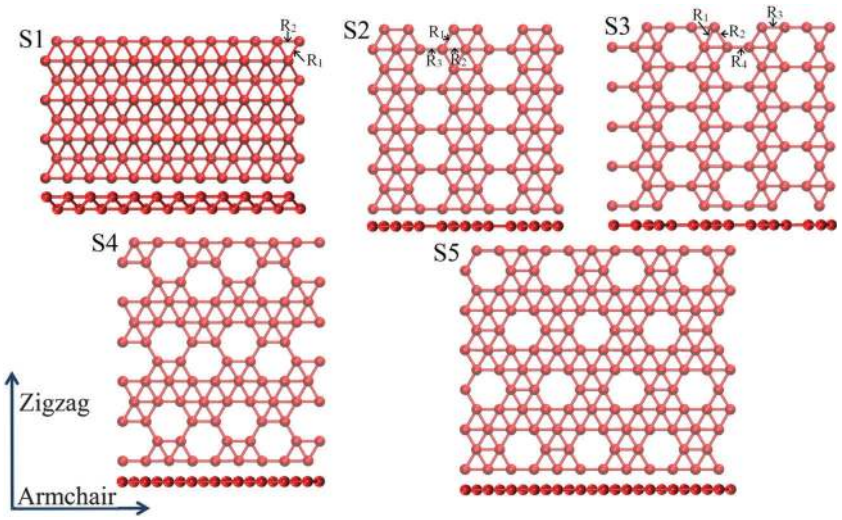

Fig. 1 Top and side views of five different borophene sheets (S1–S5) constructed in this study. The mechanical properties are studied along the armchair and zigzag directions. VMD[45] software was used to illustrate the structures.

(PBE) generalized gradient approximation exchange–correlation functional.[32] The projector augmented wave method[33] was employed with an energy cutoff of 500 eV. The conjugate gradient method was used for geometry optimizations. Periodic boundary conditions were applied in all directions and a vacuum layer of 20 Å was considered to avoid image–image interaction along the sheet thickness. For the evaluation of mechanical properties, the Brillouin zone was sampled using a $5 \times 5 \times 1$ *k*-point mesh size and for the calculation of electronic density of states we performed a single point calculation in which the Brillouin zone was sampled using a $11 \times 11 \times 1$ *k*-point mesh size using the Monkhorst–Pack mesh.[34] We applied uniaxial tension conditions to evaluate the mechanical properties of various borophene sheets. To this aim, we increased the periodic simulation box size along the loading direction in multiple steps with small engineering strain steps of 0.003. In this case, when the system is stretched in one direction, the stress on the perpendicular direction may not be zero. Depending on Poisson's ratio of the material, stretching the structure along one direction causes stretching (Poisson's ratio >0) or contracting (Poisson's ratio <0) stresses on the perpendicular directions. Since we deal with planar materials, the atoms are in contact with vacuum along the thickness. For example, for a 2D material when the structure is stretched along the armchair direction, there might be stresses along the zigzag direction. Under these conditions, to ensure accurate uniaxial stress conditions, the simulation box size along the perpendicular direction of loading was changed in a way that the stress in this direction remained negligible in comparison with that along the loading direction. The atomic positions were accordingly rescaled according to the changes in the simulation box size. Finally, the conjugate gradient method was used for geometry optimizations. It is worth noting that at every step of loading, small random displacements along the planar direction were added to the boron atom positions to avoid errors in the VASP calculation due to symmetrical atomic positions. For the *ab initio* molecular dynamics (AIMD) simulations, a Langevin thermostat was used for maintaining the temperature using a time step of 1 fs. In this case we used a $2 \times 2 \times 1$ *k*-point mesh.

3. Results and discussion

In Fig. 2, the deformation process of borophene sheets stretched along the armchair direction is depicted. We illustrated the structures at three different strain levels (ε): an energy minimized structure ($\varepsilon = 0.0$), under half of the strain at ultimate tensile strength ($\varepsilon = 0.5\varepsilon_{uts}$) and finally at the ultimate tensile strength point. For S1 borophene, due to the presence of the most regular atomic structure we observe an uniform extension of the sample along the loading direction. In this case, the buckling length decreased gradually with increasing strain level. For the S2 and S3 structures, stretching did not occur uniformly. For these sheets the bonds connecting hexagonal (in S2 borophene) or zigzag (in S3 borophene) lattices are along the loading direction and they stretched more considerably in comparison with other bonds. In S4 borophene, we also found higher deformation for the bonds connecting fully occupied hexagon lattices. Nevertheless since these bonds are not along the loading direction their deformation is closer to the other bonds in the structure. Regarding the S5 borophene, we observed higher stretching of the bonds around the hexagonal holes in the structure. Apart from the S1 films, increasing the strain levels along the loading direction decreased the periodic sheet size along the transverse direction. For small strain levels within the elastic regime, strain along the traverse direction (ε_t) with respect to the loading strain (ε_l) is acceptably constant. In this case one can evaluate Poisson's ratio by calculating $-\varepsilon_t/\varepsilon_l$. For S2 to S5 borophene films this ratio was positive meaning that the structures shrank in one direction when they were stretched along the other direction. Nevertheless, for the S1 borophene we observed a very slight increase in the periodic simulation box size in the perpendicular direction to the

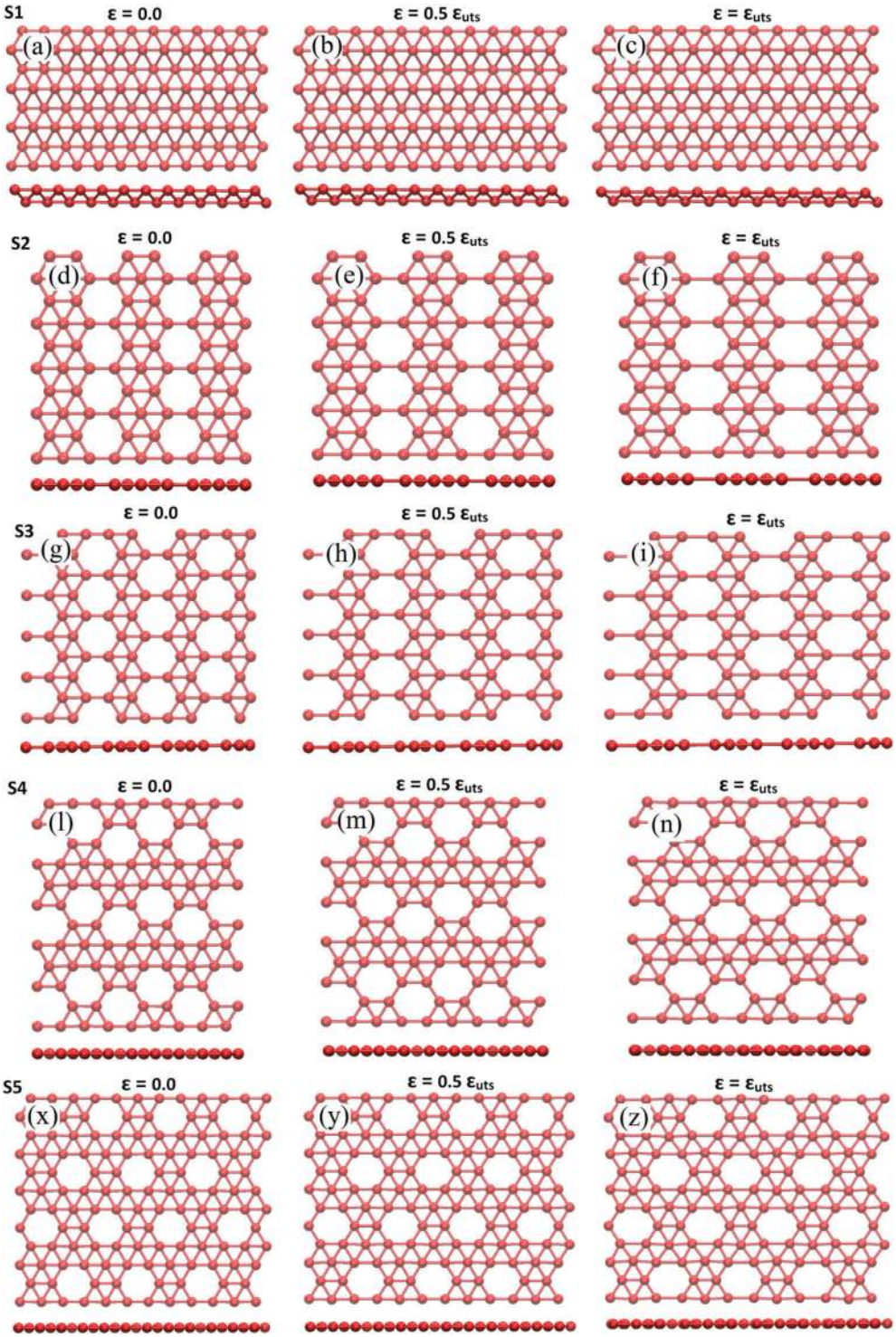

Fig. 2 Top and side view of deformation processes of single-layer borophene sheets for different strain levels (ε) with respect to strain at ultimate tensile strength (ε_{uts}).

loading direction which indicated a small negative Poisson's ratio for this structure.

Calculated uniaxial stress–strain responses of defect-free and single-layer borophene films along the armchair and zigzag loading directions are illustrated in Fig. 3. In all the cases, the stress–strain curves include an initial linear relation which is followed by a nonlinear trend up to the ultimate tensile strength at which the material yields its maximum load bearing ability. After the ultimate tensile strength point the stress decreases by increasing the strain level. The strain at which the ultimate tensile strength occurs is also an important parameter which identifies how much the material can be stretched before

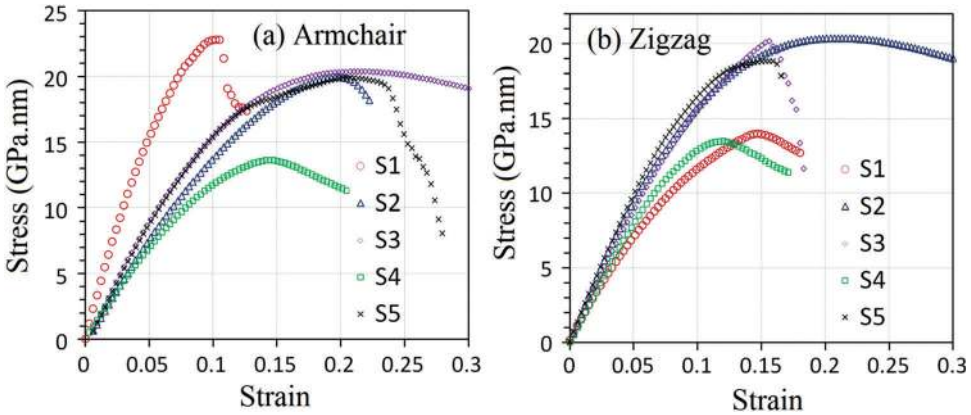

Fig. 3 Calculated uniaxial tensile stress–strain response of defect-free and single-layer borophene films along (a) armchair and (b) zigzag loading directions.

reducing its load bearing ability. The stress–strain responses of borophene sheets correlate with their atomic configurations and the way they evolve and rearrange under the loading conditions. For example, for S2 and S3 borophene films along the armchair direction, the fully occupied hexagonal or zigzag lattices are connected by single B–B bonds and therefore the stretching limit of these bonds plays a critical role in determining the ultimate tensile strength point of these structures. As is shown in Fig. 3, along the armchair direction both S2 and S3 films yield very close ultimate tensile strength points. On the other hand, when these sheets are stretched along the zigzag direction, the fully occupied hexagonal or zigzag lattices are along the loading direction and their stretching characteristics define the ultimate tensile strength point of the structure. Based on our simulations fully occupied hexagonal lattices in S2 borophene can extend more than zigzag lattices in S3 borophene.

The mechanical properties of borophene sheets predicted by our DFT calculations are summarized in Table 1. We note that the elastic modulus in the present study was evaluated by fitting a straight line to the stress–strain curves for the strain level of up to 0.006. The elastic modulus of the considered structures was similar when stretched along the armchair direction or the zigzag direction, with an exception for the S1 borophene. According to our calculations for the S1 structure, the elastic modulus was found to be 382 GPa nm along the armchair direction and 163 GPa nm along the zigzag direction. Our predictions for this borophene membrane are slightly below the previously reported elastic modulus of 398 GPa nm[16] and 389 GPa nm[35] along the armchair and 170 GPa nm[16] and 166 GPa nm[35] along the zigzag directions. This elastic modulus anisotropy for S1 graphene can be explained because of its structural features. Interestingly, the elastic modulus of the S1 structure along the zigzag direction is the lowest among the studied samples in the present study. A comparison of the strain at ultimate tensile strength values suggests the lowest value for S1 borophene stretched along the armchair direction (around 0.1). On the other hand, the S2 structure when stretched along the zigzag direction presents the highest strain at ultimate tensile strength (about 21%). A comparison of the ultimate tensile strength values suggests the highest elastic modulus of about 23 GPa nm for the S1 structure when stretched along the armchair direction. S4 borophene when stretched along the zigzag direction yields the lowest tensile strength of 13.48 GPa nm. Poisson's ratio of the S1 structure was found to be negative and close to zero. Poisson's ratio of the other four structures ranged from about 0.1 to 0.25. We found that Poisson's ratio of borophene films is convincingly independent of the loading direction. We note that according to recent theoretical predictions,[35,36] the S1 borophene film present phonon instability likely to MoS_2.[35] It was concluded that the S1 borophene lattice may exhibit instability against long-wavelength transversal waves.[35] The investigation of phonon instability of considered borophene films under different loading conditions is therefore an interesting topic for future studies.

Fig. 4 shows the samples of B–B bond length evolution during the uniaxial stretching of S1, S2 and S3 borophene sheets along the armchair direction. As expected, the bonds that were along the direction of stretching were gradually elongated with increasing strain levels. For all of the studied sheets, we found that the bonds that were not along the direction of stretching either decreased in length (*e.g.* Fig. 4a, R_2 bond) or remained almost similar to their

Table 1 Mechanical properties of borophene sheets, *Y*, *P*, STS and UTS depict the elastic modulus, Poisson's ratio, strain at ultimate tensile strength point and ultimate tensile strength, respectively. Stress units are in GPa nm

Structure	$Y_{armchair}$	Y_{zigzag}	P	$STS_{armchair}$	STS_{zigzag}	$UTS_{armchair}$	UTS_{zigzag}
S1	382	163	−0.01	0.105	0.145	22.8	14
S2	190	210	0.18	0.2	0.21	19.97	20.38
S3	208	205	0.11	0.21	0.155	19.91	20.18
S4	186	167	0.26	0.14	0.12	15.65	13.48
S5	214	217	0.2	0.21	0.16	14.84	18.83

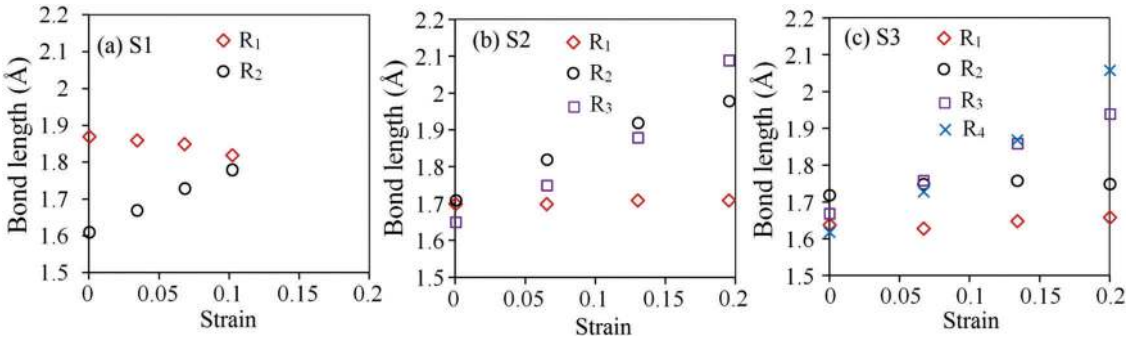

Fig. 4 Samples of variation of bond lengths for various strain levels for structures (a) S1, (b) S2 and (c) S3, uniaxially loaded along the armchair direction. Different bonds R_1, R_2, R_3 and R_4 for studied systems are depicted in Fig. 1.

initial values (*e.g.* Fig. 4b, R_1 bond) with increasing strain levels. In the cases of S2, S3, S4 and S5 borophene, membranes non-identical to stretching were observed for different bond types that were along the direction of stretching. For example, for the S2 sheet, the R_3 bond (as depicted in Fig. 1) was stretched at a higher rate than the R_2 bond, in a similar way, for the S3 sheet, the R_4 bond was stretched at a higher rate than the R_3 bond. These can probably be explained by the higher propensity of the two center-two electron (c2–2e) bonds (R_3 in the case of S2 and R_4 in the case of S3) to be stretched easily as compared to the three center-two electron (3c–2e) bonds (R_2 in the case of S2 and R_3 in the case of S3).

All five considered borophene sheets at different strain levels up to the tensile strength point were selected for electronic density of state (DOS) calculation. Fig. 5 illustrates the samples of acquired DOS curves for borophene films elongated along the armchair direction. As can be observed, in the calculated total DOS for the relaxed and uniaxially loaded systems, at the zero state energy (Fermi level) the DOS is not zero, which consequently demonstrates metallic behaviour. For the S1 borophene, we found that upon stretching, the total DOS for the valence/conduction band around the Fermi level is increased. On the other hand, for the rest of the considered borophene films we observed that during the elongation the total DOS around the Fermi level slightly decreases. Nevertheless, according to our findings, one cannot open a band gap by stretching borophene films.

Like all other known materials, experimentally fabricated borophene sheets are expected not to be perfect and different types of defects may exist in borophene lattices. Defects in materials influence both physical and chemical properties and in some cases it may substantially affect the electronic properties.[37–39] Defects in 2D materials such as graphene are formed mainly during the fabrication process. Despite the high thermal stability of graphene, with a melting point of 4510 K,[40] crystal growth during chemical vapour deposition (CVD) forms various types of defects in graphene.[39,41] Since the thermal stability of borophene sheets is considerably lower than graphene, the existence of defects in experimentally fabricated borophene sheets is therefore expected to be common. The presence of defects can naturally affect the mechanical properties of 2D materials. In order to understand the role of defects in the mechanical properties of borophene sheets, we introduced point defects by gradually removing 1, 2, 3 or 4 atoms from the structures. We note that more than 10 different

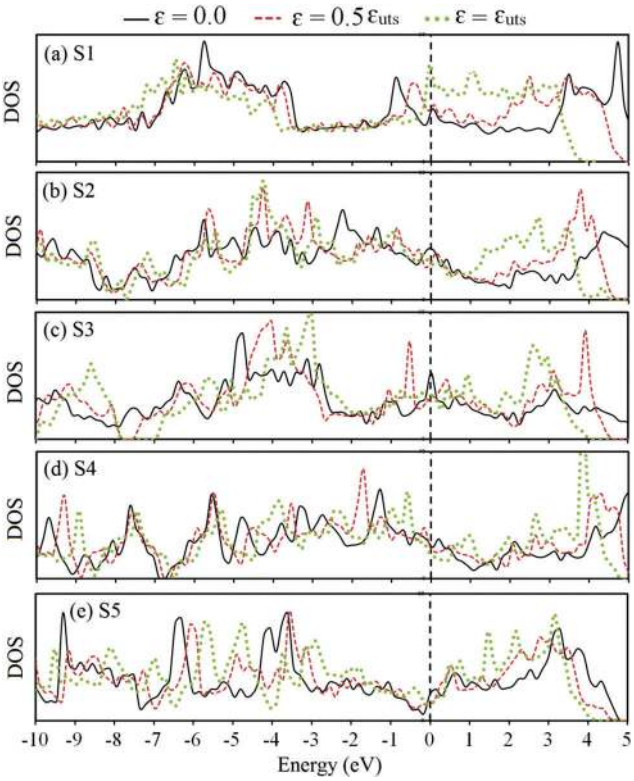

Fig. 5 Total electronic density of states (DOS) for borophene structures elongated along the armchair directions at different strains (ε) with respect to the strain at ultimate tensile strength (ε_{uts}).

borophene films have been predicted theoretically[29] or fabricated experimentally.[16,17] The difference in these boron films is due to the regular pattern of the removed boron atoms in the unit-cell. This way, for the modelling of defective borophene films we accordingly removed the boron atoms randomly such that the obtained structure is not symmetrical and is similar to the other borophene films. After removing few boron atoms for every structure, we performed energy minimization to obtain the relaxed structure. In Fig. 6, the top views of the minimized highly defective borophene sheets are illustrated. We observed remarkable out of plane deflection of S1 sheets whereas the other structures are kept planar. In order to analyze the correlation between the electronic and mechanical properties of defective

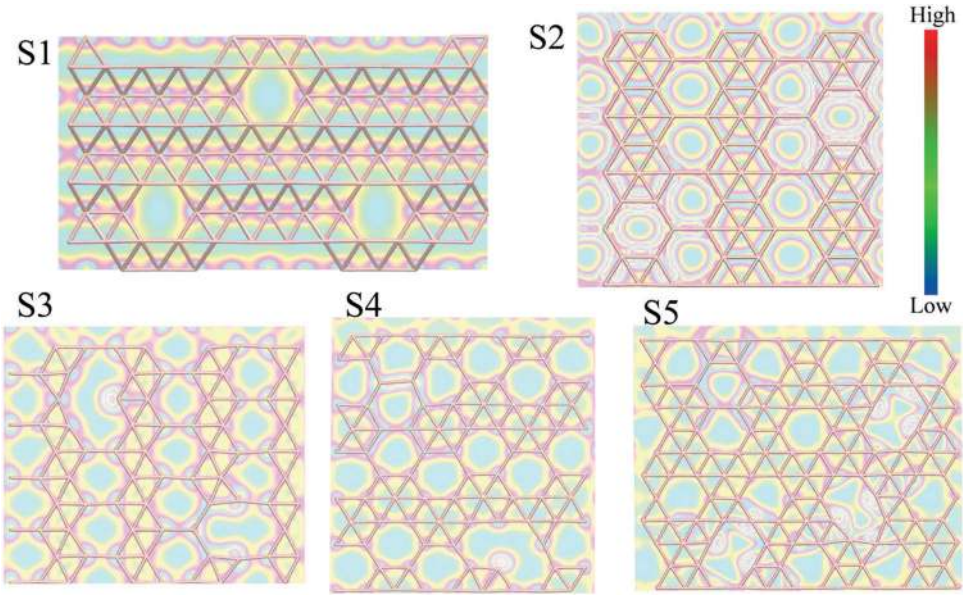

Fig. 6 Top view of various minimized defective borophene sheets. The contour illustrates partial charges density around the Fermi energy. For the S1 sheet, the charge density is plotted for the atoms that are placed on the botton atomic plane.

structures, we plotted the partial charge density around the Fermi energy for the borophene films with highest defect concentrations as shown in Fig. 6. The charge localization effect determines the elastic properties of the nanostructures. Higher charge localization leads to stronger bonding energy and consequently higher mechanical stability.[42] The highest localized charges are observed between B–B bonds for the S1 structure resulting in the highest elastic modulus for this structure. The lowest charge density between B–B bonds are indicated for S2 borophene. Because of the similar charge distributions for S3, S4, and S5 structures the correlation between charge density and the elastic modulus is not trivial. However, all these structures present a close elastic modulus. In addition, we conducted electronic density of state calculation for constructed defective borophene sheets. Our calculated total DOS confirms that in all cases, the structures present metallic behaviour as indicated by the lack of any band gaps in the DOS.

After obtaining the minimized structures, borophene films were subjected to loading strains to evaluate the elastic modulus. Since the elastic modulus of S1 borophene is highly anisotropic, in this case we calculated the elastic modulus along both armchair and zigzag directions. The elastic modulus of borophene sheets as a function of point defect concentration is illustrated in Fig. 7. Based on our simulations, the elastic modulus of considered borophene films along the armchair direction decreased almost linearly with increasing defect concentration. It is worth noting that based on classical molecular dynamics simulations it was predicted that the elastic modulus of graphene decreases also linearly with increasing defect concentrations[43,44] and such a relation was found to be consistent also for amorphized graphene.[44] The decreasing trends in the elastic modulus and tensile strength of a covalently bonded material by increasing the defect concentration is expected since the loss of an atom

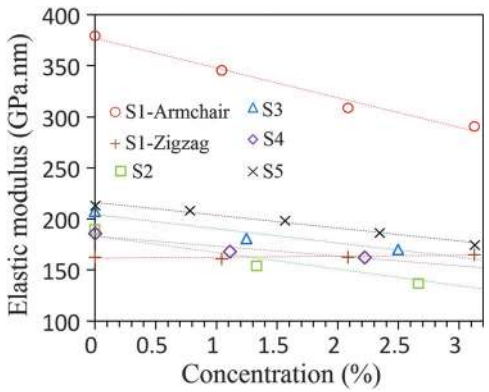

Fig. 7 Elastic modulus of borophene sheets as a function point defect concentration.

not only removes bonds that are involved in the load transfer but also causes stress concentrations which consequently reduce the mechanical strength. Interestingly, our first principles calculation reveals that the elastic modulus of the S1 structure along the zigzag direction rather slightly increases with increasing defect concentration. To understand the mechanism behind such an unexpected trend, we should remember that sheets S2 to S5 are nothing but structure S1 in which some atoms are removed with special patterns leading to the formation of planar films. Based on our results discussed earlier, the elastic modulus of all these structures is higher than that of the original S1 sheet along the zigzag direction. So one can conclude that by increasing the defect concentrations in S1 borophene its structure will approach other planar and pristine borophene sheets. Since the elastic modulus along zigzag direction for these borophene sheets is higher than that for the S1 borophene along the zigzag direction, by increasing the defect concentration the S1 borophene presents

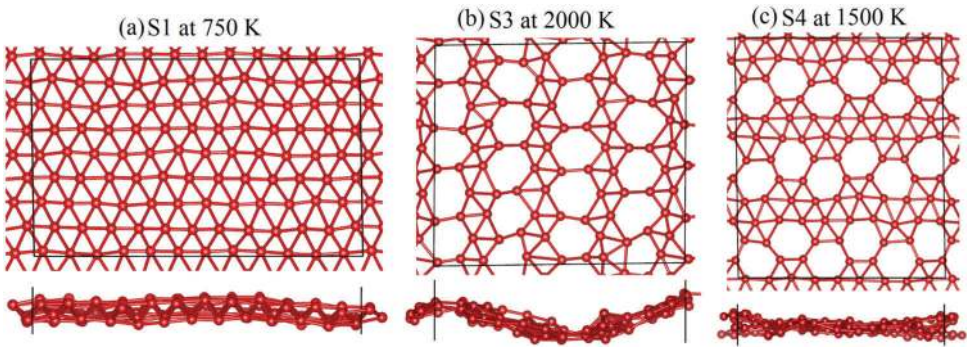

Fig. 8 Thermal stability of borophene films. Snapshots of S1, S3 and S4 borophene sheets at different temperatures obtained using AIMD calculations for 5 ps. VESTA[46] package was utilized to illustrate these structures.

a slightly higher elastic modulus along the zigzag direction. It is worth noting that such a trend is predicted to be valid only for small defect concentrations and after a point, a further increase of the defect concentrations will result in a decrease in the elastic modulus. For the defective films, we also calculated Poisson's ratio and found that by increasing the defect concentration Poisson's ratio does not change considerably. Only for the S1 borophene, we found that by increasing the defect concentration Poisson's ratio become slightly positive. This finding was expectable because of the fact that the S1 structure by increasing the defect concentration approaches the other borophene films which present positive Poisson's ratio.

Thermal stability is a desirable quality in nanomaterials of practical use. In this work we also studied the thermal stabilities of the five borophene structures at high temperature using AIMD simulations. 5 picoseconds of simulations were performed for all the structures. The S1 structure remained intact at the end of the simulation at $T = 750$ K. It was partly disintegrated at $T = 1000$ K and $T = 1500$ K and completely disintegrated at $T = 2000$ K. The S2 structure was completely disintegrated at $T = 3000$ K but only partially at $T = 2000$ K. S3 and S5 structures were intact at $T = 2000$ K but disintegrated at $T = 3000$ K. The S4 structure was intact at $T = 1500$ K but disintegrated at $T = 2000$ K. In Fig. 8 samples of S1, S2 and S4 borophene sheets at different temperatures obtained using AIMD calculations for 5 ps are illustrated. Despite considerable deformation of the structures due to thermal fluctuations, the chemical bonds were intact, which confirms the stability of the structures. Putting together, it can be concluded that the S1 structure is the least thermally stable among all the structures and none of the structures can withstand a high temperature like $T = 3000$ K.

4. Summary

We performed extensive first-principles density functional theory calculations to provide a general viewpoint concerning the mechanical properties of five different borophene sheets. To this aim, we applied uniaxial tension conditions to study the mechanical properties of borophene sheets. For all the considered borophene structures, we analyzed the effects of the loading direction and point vacancy on the mechanical response. Our first-principles modelling revealed that borophene films depending on the boron atom arrangements and the loading direction can yield a remarkable elastic modulus in the range of 163–382 GPa nm and a high ultimate tensile strength from 14 GPa nm to around 22.8 GPa nm at a corresponding strain from 0.1 to 0.21. While the elastic modulus and ultimate tensile points of borophene sheets were found to be anisotropic, their Poisson's ratios were predicted to be almost independent of the loading direction. Based on our modelling results Poisson's ratio of borophene films can vary from −0.01 up to around 0.26. Our simulation results for all relaxed and uniaxially strained systems up to the ultimate tensile strength point suggest that borophene sheets present metallic behaviour as indicated by the lack of band gap opening in the electronic DOS. In addition, in order to understand the intensity of defect formation and its effect on the mechanical properties of borophene sheets, we studied the elastic modulus of borophene membranes with different point defect concentrations. We found that the elastic modulus of the considered borophene films along the armchair direction decreases almost linearly by increasing the defect concentration. Interestingly, our DFT calculations revealed that the elastic modulus of a particular borophene structure along the zigzag direction slightly increases with increasing defect concentration. *Ab initio* molecular dynamics simulations suggest that borophene films depending on their atomic arrangements can withstand temperatures from 750 K to 2000 K. The information provided by the present investigation can be useful to validate the parameterization of force fields for simulation of borophene films at a larger scale using the classical molecular dynamics method.

Acknowledgements

BM, OR and TR greatly acknowledge the financial support by European Research Council for COMBAT project (Grant number 615132).

References

1 K. S. Novoselov, A. K. Geim, S. V Morozov, D. Jiang, Y. Zhang and S. V Dubonos, *et al.* Electric field effect in atomically thin carbon films, *Science*, 2004, **306**, 666–669, DOI: 10.1126/science.1102896.
2 A. K. Geim and K. S. Novoselov, The rise of graphene, *Nat. Mater.*, 2007, **6**, 183–191, DOI: 10.1038/nmat1849.

3 A. H. Castro Neto, N. M. R. Peres, K. S. Novoselov, A. K. Geim and F. Guinea, The electronic properties of graphene, *Rev. Mod. Phys.*, 2009, **81**, 109–162, DOI: 10.1103/RevModPhys.81.109.
4 C. Lee, X. Wei, J. W. Kysar and J. Hone, Measurement of the Elastic Properties and Intrinsic Strength of Monolayer Graphene, *Science*, 2008, **321**, 385–388, DOI: 10.1126/science.1157996.
5 A. A. Balandin, Thermal properties of graphene and nanostructured carbon materials, *Nat. Mater.*, 2011, **10**, 569–581, DOI: 10.1038/nmat3064.
6 Y. Kubota, K. Watanabe, O. Tsuda and T. Taniguchi, Deep ultraviolet light-emitting hexagonal boron nitride synthesized at atmospheric pressure, *Science*, 2007, **317**, 932–934, DOI: 10.1126/science.1144216.
7 L. Song, L. Ci, H. Lu, P. B. Sorokin, C. Jin and J. Ni, *et al.* Large scale growth and characterization of atomic hexagonal boron nitride layers, *Nano Lett.*, 2010, **10**, 3209–3215, DOI: 10.1021/nl1022139.
8 G. Algara-Siller, N. Severin, S. Y. Chong, T. Björkman, R. G. Palgrave and A. Laybourn, *et al.* Triazine-based graphitic carbon nitride: A two-dimensional semiconductor, *Angew. Chem., Int. Ed.*, 2014, **53**, 7450–7455, DOI: 10.1002/anie.201402191.
9 B. Aufray, A. Kara, Ś. Vizzini, H. Oughaddou, C. Ĺandri and B. Ealet, *et al.* Graphene-like silicon nanoribbons on Ag(110): A possible formation of silicene, *Appl. Phys. Lett.*, 2010, **96**, 183102, DOI: 10.1063/1.3419932.
10 P. Vogt, P. De Padova, C. Quaresima, J. Avila, E. Frantzeskakis and M. C. Asensio, *et al.*, Silicene: Compelling experimental evidence for graphenelike two-dimensional silicon, *Phys. Rev. Lett.*, 2012, **108**, 155501, DOI: 10.1103/PhysRevLett.108.155501.
11 E. Bianco, S. Butler, S. Jiang, O. D. Restrepo, W. Windl and J. E. Goldberger, Stability and exfoliation of germanane: A germanium graphane analogue, *ACS Nano*, 2013, **7**, 4414–4421, DOI: 10.1021/nn4009406.
12 F. Zhu, W. Chen, Y. Xu, C. Gao, D. Guan, C. Liu, Epitaxial Growth of Two-Dimensional Stanene, 2015, arXiv:10.1038/nmat4384, **1**, 20.
13 A. K. Geim and I. V Grigorieva, Van der Waals heterostructures, *Nature*, 2013, **499**, 419–425, DOI: 10.1038/nature12385.
14 Q. H. Wang, K. Kalantar-Zadeh, A. Kis, J. N. Coleman and M. S. Strano, Electronics and optoelectronics of two-dimensional transition metal dichalcogenides, *Nat. Nanotechnol.*, 2012, **7**, 699–712, DOI: 10.1038/nnano.2012.193.
15 B. Radisavljevic, A. Radenovic, J. Brivio, V. Giacometti and A. Kis, Single-layer MoS$_2$ transistors., *Nat. Nanotechnol.*, 2011, **6**, 147–150, DOI: 10.1038/nnano.2010.279.
16 A. J. Mannix, X.-F. Zhou, B. Kiraly, J. D. Wood, D. Alducin and B. D. Myers, *et al.*, Synthesis of borophenes: Anisotropic, two-dimensional boron polymorphs, *Science*, 2015, **350**, 1513–1516, DOI: 10.1126/science.aad1080.
17 B. Feng, J. Zhang, Q. Zhong, W. Li, S. Li and H. Li, *et al.*, Experimental realization of two-dimensional boron sheets, *Nat. Chem.*, 2016, **8**, 563–568, DOI: 10.1038/nchem.2491.
18 X. F. Zhou, X. Dong, A. R. Oganov, Q. Zhu, Y. Tian and H. T. Wang, Semimetallic two-dimensional boron allotrope with massless Dirac fermions, *Phys. Rev. Lett.*, 2014, **112**, 085502, DOI: 10.1103/PhysRevLett.112.085502.
19 Z. Zhang, Y. Yang, G. Gao and B. I. Yakobson, Two-Dimensional Boron Monolayers Mediated by Metal Substrates, *Angew. Chem.*, 2015, **127**, 13214–13218, DOI: 10.1002/ange.201505425.
20 A. A. Khatibi and B. Mortazavi, A Study on the Nanoindentation Behaviour of Single Crystal Silicon Using Hybrid MD-FE Method, *Adv. Mater. Res.*, 2008, **32**, 259–262, DOI: 10.4028/www.scientific.net/AMR.32.259.
21 B. Mortazavi, A. A. Khatibi and C. Politis, Molecular dynamics investigation of loading rate effects on mechanical-failure behaviour of FCC metals, *J. Comput. Theor. Nanosci.*, 2009, **6**, 644–652, DOI: 10.1166/jctn.2009.1087.
22 Q. Peng, L. Han, X. Wen, S. Liu, Z. Chen and J. Lian, *et al.*, Mechanical properties and stabilities of α-boron monolayers., *Phys. Chem. Chem. Phys.*, 2015, **17**, 2160–2168, DOI: 10.1039/c4cp04050c.
23 S. N. Shirodkar, U. V. Waghmare, T. S. Fisher and R. Grau-Crespo, Engineering the electronic bandgaps and band edge positions in carbon-substituted 2D boron nitride: A first-principles investigation, *Phys. Chem. Chem. Phys.*, 2015, **17**, 13547–13552, DOI: 10.1039/c5cp01680k.
24 M. M. Islam, A. Ostadhossein, O. Borodin, A. T. Yeates, W. W. Tipton and R. G. Hennig, *et al.* ReaxFF molecular dynamics simulations on lithiated sulfur cathode materials, *Phys. Chem. Chem. Phys.*, 2015, **17**, 3383–3393, DOI: 10.1039/C4CP04532G.
25 A. Ostadhossein, E. D. Cubuk, G. A. Tritsaris, E. Kaxiras, S. Zhang and A. C. T. van Duin, Stress effects on the initial lithiation of crystalline silicon nanowires: reactive molecular dynamics simulations using ReaxFF, *Phys. Chem. Chem. Phys.*, 2015, **17**, 3832–3840, DOI: 10.1039/C4CP05198J.
26 M. Q. Le and D. T. Nguyen, Atomistic simulations of pristine and defective hexagonal BN and SiC sheets under uniaxial tension, *Mater. Sci. Eng., A*, 2014, **615**, 481–488, DOI: 10.1016/j.msea.2014.07.109.
27 M. Q. Le and D. T. Nguyen, The role of defects in the tensile properties of silicene, *Appl. Phys. A: Mater. Sci. Process.*, 2014, **118**, 1437–1445, DOI: 10.1007/s00339-014-8904-3.
28 M. Mirnezhad, R. Ansari, H. Rouhi, M. Seifi and M. Faghihnasiri, Mechanical properties of two-dimensional graphyne sheet under hydrogen adsorption, *Solid State Commun.*, 2012, **152**, 1885–1889, DOI: 10.1016/j.ssc.2012.07.024.
29 Z. Zhang, Y. Yang, G. Gao and B. I. Yakobson, Two-Dimensional Boron Monolayers Mediated by Metal Substrates, *Angew. Chem.*, 2015, **127**, 13214–13218, DOI: 10.1002/ange.201505425.
30 G. Kresse and J. Furthmüller, Efficiency of ab-initio total energy calculations for metals and semiconductors using a plane-wave basis set, *Comput. Mater. Sci.*, 1996, **6**, 15–50, DOI: 10.1016/0927-0256(96)00008-0.
31 G. Kresse and J. Furthmüller, Efficient iterative schemes for *ab initio* total-energy calculations using a plane-wave basis set, *Phys. Rev. B: Condens. Matter Mater. Phys.*, 1996, **54**, 11169–11186, DOI: 10.1103/PhysRevB.54.11169.

32 J. Perdew, K. Burke and M. Ernzerhof, Generalized Gradient Approximation Made Simple, *Phys. Rev. Lett.*, 1996, **77**, 3865–3868, DOI: 10.1103/PhysRevLett.77.3865.

33 G. Kresse, From ultrasoft pseudopotentials to the projector augmented-wave method, *Phys. Rev. B: Condens. Matter Mater. Phys.*, 1999, **59**, 1758–1775, DOI: 10.1103/PhysRevB.59.1758.

34 D. J. Chadi and M. L. Cohen, Special points in the brillouin zone, *Phys. Rev. B: Solid State*, 1973, **8**, 5747–5753, DOI: 10.1103/PhysRevB.8.5747.

35 H. Wang, Q. Li, Y. Gao, F. Miao, X. F. Zhou and X. G. Wan, Strain effects on borophene: ideal strength, negative Possion's ratio and phonon instability, *New J. Phys.*, 2016, **18**, 73016, http://stacks.iop.org/1367-2630/18/i=7/a=073016.

36 B. Peng, H. Zhang, H. Shao, Y. Xu, R. Zhang and H. Zhu, The electronic, optical and thermodynamic properties of borophene from first-principles calculations, *J. Mater. Chem. C*, 2016, **4**, 3592–3598, DOI: 10.1039/C6TC00115G.

37 A. Cresti, N. Nemec, B. Biel, G. Niebler, F. Triozon and G. Cuniberti, *et al.*, Charge transport in disordered graphene-based low dimensional materials, *Nano Res.*, 2008, **1**, 361–394, DOI: 10.1007/s12274-008-8043-2.

38 A. Lherbier, S. M.-M. Dubois, X. Declerck, Y.-M. Niquet, S. Roche and J.-C. Charlier, Transport properties of graphene containing structural defects, *Phys. Rev. B: Condens. Matter Mater. Phys.*, 2012, **86**, 075402, DOI: 10.1103/PhysRevB.86.075402.

39 F. Banhart, J. Kotakoski and A. V. Krasheninnikov, Structural defects in graphene, *ACS Nano*, 2011, **5**, 26–41, DOI: 10.1021/nn102598m.

40 J. H. Los, K. V. Zakharchenko, M. I. Katsnelson and A. Fasolino, Melting temperature of graphene, *Phys. Rev. B: Condens. Matter Mater. Phys.*, 2015, **91**, 045415, DOI: 10.1103/PhysRevB.91.045415.

41 J. Kotakoski, A. V. Krasheninnikov, U. Kaiser and J. C. Meyer, From point defects in graphene to two-dimensional amorphous carbon, *Phys. Rev. Lett.*, 2011, **106**, 105505, DOI: 10.1103/PhysRevLett.106.105505.

42 C. Gatti, Chemical bonding in crystals: New directions, *Z. Kristallogr.*, 2005, **220**, 399–457, DOI: 10.1524/zkri.220.5.399.65073.

43 B. Mortazavi and S. Ahzi, Thermal conductivity and tensile response of defective graphene: A molecular dynamics study, *Carbon*, 2013, **63**, 460–470, DOI: 10.1016/j.carbon.2013.07.017.

44 B. Mortazavi, Z. Fan, L. F. C. Pereira, A. Harju and T. Rabczuk, Amorphized graphene: A stiff material with low thermal conductivity, *Carbon*, 2016, **103**, 318–326, DOI: 10.1016/j.carbon.2016.03.007.

45 W. Humphrey, A. Dalke and K. Schulten, VMD: Visual molecular dynamics, *J. Mol. Graphics*, 1996, **14**, 33–38, DOI: 10.1016/0263-7855(96)00018-5.

46 K. Momma and F. Izumi, VESTA 3 for three-dimensional visualization of crystal, volumetric and morphology data, *J. Appl. Crystallogr.*, 2011, **44**, 1272–1276, DOI: 10.1107/S0021889811038970.